Chemistry & Biology
Article

# Bisubstrate Adenylation Inhibitors of Biotin Protein Ligase from *Mycobacterium tuberculosis*

Benjamin P. Duckworth,[1] Todd W. Geders,[2] Divya Tiwari,[3] Helena I. Boshoff,[4] Paul A. Sibbald,[1] Clifton E. Barry, III,[4] Dirk Schnappinger,[3] Barry C. Finzel,[2] and Courtney C. Aldrich[1,*]
[1]Center for Drug Design, University of Minnesota, Minneapolis, MN 55455, USA
[2]Department of Medicinal Chemistry, University of Minnesota, Minneapolis, MN 55455, USA
[3]Department of Microbiology and Immunology, Weill Cornell Medical College, New York, NY 10065, USA
[4]Tuberculosis Research Section, National Institute of Allergy and Infectious Diseases, Bethesda, MD 20892, USA
*Correspondence: aldri015@umn.edu
DOI 10.1016/j.chembiol.2011.08.013

## SUMMARY

**The mycobacterial biotin protein ligase (*Mt*BPL) globally regulates lipid metabolism in *Mtb* through the posttranslational biotinylation of acyl coenzyme A carboxylases involved in lipid biosynthesis that catalyze the first step in fatty acid biosynthesis and pyruvate coenzyme A carboxylase, a gluconeogenic enzyme vital for lipid catabolism. Here we describe the design, development, and evaluation of a rationally designed bisubstrate inhibitor of *Mt*BPL. This inhibitor displays potent subnanomolar enzyme inhibition and antitubercular activity against multidrug resistant and extensively drug resistant *Mtb* strains. We show that the inhibitor decreases in vivo protein biotinylation of key enzymes involved in fatty acid biosynthesis and that the antibacterial activity is *Mt*BPL dependent. Additionally, the gene encoding BPL was found to be essential in *M. smegmatis*. Finally, the X-ray cocrystal structure of inhibitor bound *Mt*BPL was solved providing detailed insight for further structure-activity analysis. Collectively, these data suggest that *Mt*BPL is a promising target for further antitubercular therapeutic development.**

## INTRODUCTION

Tuberculosis (TB) caused by the bacterium *Mycobacterium tuberculosis* (*Mtb*) continues to burden human health on a global scale. Despite an impressive amount of effort directed at eradicating tuberculosis, TB is still the second leading cause of mortality among infectious diseases superseded only by HIV. The emergence of multidrug-resistant (MDR) and extensively drug-resistant (XDR) TB strains coupled with the high incidence of HIV-TB coinfection and the lack of any new approved chemotherapeutic agents for TB in over four decades, demands the development of new antitubercular agents, ideally with novel mechanisms of action, to combat this devastating pathogen.

Fatty acid biosynthesis is a validated pathway for antitubercular drug discovery, and the first-line agent isoniazid inhibits the type II fatty acid synthase (FAS-II) in *Mtb* (Slayden et al., 2000; Timm et al., 2003). Acyl coenzyme A carboxylases (ACCs) catalyze the first committed step in fatty acid biosynthesis through synthesis of the monomeric malonyl-CoA building blocks. However, unlike most bacteria that encode for a single ACC complex, *Mtb* encodes for multiple ACCs responsible for the biosynthesis of malonyl coenzyme A (CoA), (methyl)malonyl CoA, and (C22–C24) malonyl CoA for construction of the structurally diverse lipids in *Mtb*, including simple linear fatty acids, methyl-branched lipids, and mycolic acids (Gago et al., 2006; Kurth et al., 2009; Portevin et al., 2005). In order for the ACCs to become functionally active, the biotin-carboxylase carrier protein (BCCP) domains of these proteins must be posttranslationally modified to their active holo biotinylated form by a biotin protein ligase (BPL) encoded by *birA* in *Mtb* (*Mt*BPL) (Purushothaman et al., 2008). The biotin serves as the cofactor that mediates carboxyl group transfer onto the acetyl CoA substrates. In addition to fatty acid biosynthesis, fatty acid degradation is also an essential process, and mycobacteria are thought to be primarily lipolytic in vivo deriving their energy via fatty acid catabolism (Timm et al., 2003). *Mt*BPL may also play a key role in fatty acid degradation, because this enzyme is also responsible for biotinylation of the BCCP domain of pyruvate carboxylase, which can channel oxaloacetate to the phosphoenolpyruvate carboxykinase, a gluconeogenic enzyme that is essential for growth on fatty acids and critical for mycobacterial pathogenesis (Marrero et al., 2010). *Mt*BPL thus globally regulates lipid metabolism and represents an attractive target for development of new antitubercular agents.

There are two classes of biotin protein ligases (BPLs): the monofunctional enzymes represented by the BPL from *Pyrococcus horikoshii* (*Ph*BPL), which solely catalyze posttranslational biotinylation, and the bifunctional enzymes represented by the prototypical BPL from *Escherichia coli* (*Ec*BPL), which also act as transcriptional repressors (Brown et al., 2004; Chapman-Smith and Cronan, 1999). Recent biochemical characterization of the BPL from *Mtb* (*Mt*BPL) has revealed it to be a monofunctional enzyme that exists as a monomer in both the unliganded apo-and holo-forms as well as in the biotinyl adenylate (Bio-AMP, **2**) liganded form (Purushothaman et al., 2008). BPLs catalyze the transfer of biotin onto a conserved lysine residue of the biotin-carboxylase carrier protein (BCCP) domain of ACCs. This reaction is accomplished in two steps: in the first-half reaction, BPLs bind biotin (**1**, Figure 1A) and ATP and

 

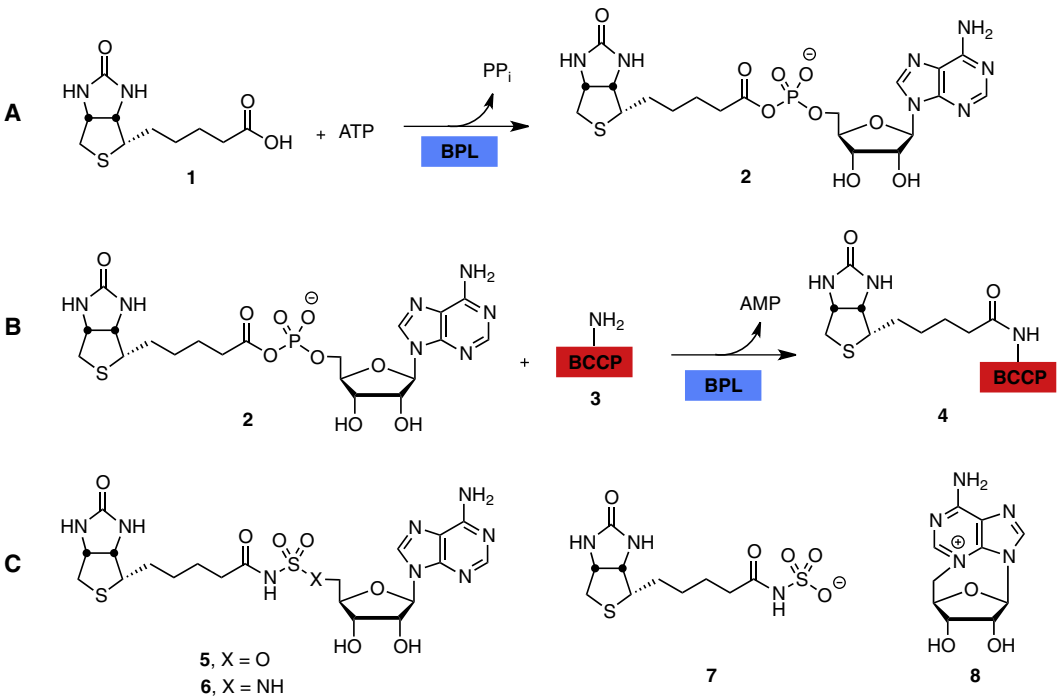


**Figure 1. Enzyme Reaction Catalyzed by BPL**
(A) First half-reaction to form biotin adenylate.
(B) Second half-reaction involving transfer of biotin to acetyl CoA carboxylases.
(C) Bisubstrate inhibitors of BPL and degradation products of **5**.
See also Figure S1.

catalyze the nucleophilic attack of the biotin carboxylate onto the α-phosphate of ATP to yield the acyl-adenylate Bio-AMP **2** (Figure 1A) and pyrophosphate. In the second-half reaction, BPLs transfer biotin from Bio-AMP **2** onto a conserved lysine residue within the BCCP domain **3** to provide biotinylated-BCCP **4** (Figure 1B). The bisubstrate inhibitor **5** (Figure 1C) has been described, which mimics the intermediate acyl-adenylate Bio-AMP **2** by replacement of the labile acylphosphate linkage in Bio-AMP **2** with the bioisosteric acylsulfamate moiety (Brown and Beckett, 2005; Brown et al., 2004). Interestingly, the bisubstrate inhibitor **5** was found to bind 1.4-fold more weakly to *Ec*PBL than the single substrate biotin, suggesting the acylsulfamate was a poor isostere for the native acylphosphate linkage.

Here we describe the design, synthesis, biochemical, structural, and biological evaluation of a bisubstrate inhibitor of *Mt*BPL that we term Bio-AMS (**6**, Figure 1C) which binds more than 1700-fold more tightly than biotin and possesses potent and selective antimicrobial activity against MDR- and XDR-TB strains of *Mtb*. We used *M. smegmatis* to confirm that the BPL-encoding gene, *birA*, is essential as well as to assess susceptibility of *Mt*BPL to inhibition in vivo. Support for the designed mechanism of action is provided using a combination of proteomic profiling and genetic studies. Finally, we describe the detailed molecular interactions present between *Mt*BPL and Bio-AMS that establish the molecular basis for potent inhibition and provides a framework for future structure-aided drug design.

## RESULTS

### Inhibitor Design and Synthesis

Bisubstrate inhibitors that mimic acyl-adenylate reaction intermediates typically bind much more tightly than the individual substrates owing to the large number of interactions between the inhibitor and both substrate binding sites (Ferreras et al., 2005; Somu et al., 2006). The reported lack of potency of **5** toward *Ec*BPL is surprising (Brown and Beckett, 2005), so we synthesized this compound as described in Supplemental Experimental Procedures. We immediately observed that it is chemically unstable and decomposes through cyclonucleoside formation to afford *N*-biotinylsulfamic acid **7** (Figure 1C) and 3,5′-cyclo-5′-deoxyadenosine **8** (experimental details and complete characterization are found in the Supplemental Information). We hypothesized that a more stable compound would result if the 5′-oxygen atom in sulfamate **5** were replaced with a nitrogen atom of sulfamide **6** as a result of the decreased nucleofugality of the sulfamide (Broeckaert et al., 2008). Compound **6** (Bio-AMS) was synthesized, and as predicted, it did not undergo cyclonucleoside formation. Because of its improved stability, Bio-AMS represents an excellent probe to chemically validate *Mt*BPL as a target for antitubercular therapeutic development.

### Biochemical Evaluation of Bio-AMS

We next evaluated Bio-AMS in a kinetic continuous coupled assay with 250 nM *Mt*BPL to determine the concentration-response curve for inhibition of *Mt*BPL at fixed saturating

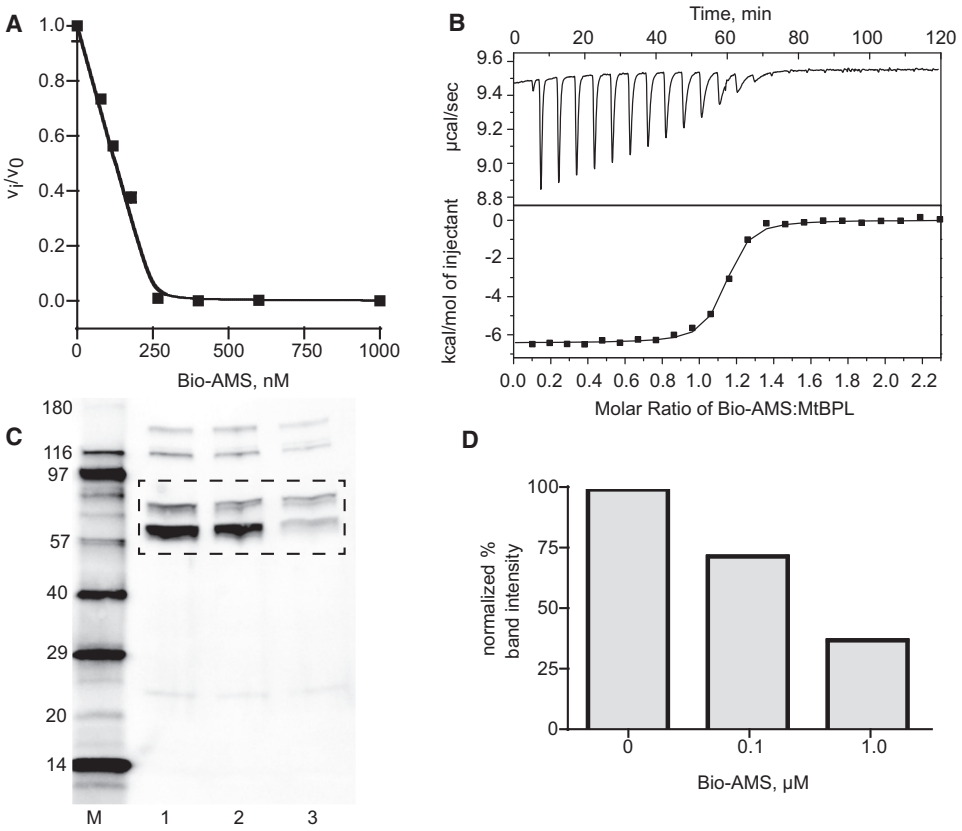


**Figure 2. In Vitro Analysis and Mechanism of Action Studies of Bio-AMS Inhibitor**

(A) Dose-response of *Mt*BPL with inhibitor Bio-AMS. $v_i$ and $v_0$ are velocities of inhibitor and DMSO treated samples, respectively.

(B) Competitive ITC trace of a solution of Bio-AMS (200 µM) in 10 mM Tris (pH 7.5), 200 mM KCl, and 2.5 mM $MgCl_2$ titrated into a solution of *Mt*BPL (20 µM) and biotin (150 µM) in the same buffer.

(C) Western blot analysis of biotinylated protein levels in lysates from *Mtb* H37Rv cells treated with varying concentrations of Bio-AMS. Lane M: biotinylated molecular weight marker; Lane 1, DMSO-treated MTB cells; Lane 2, *Mtb* cells treated with 0.1 µM Bio-AMS; Lane 3: *Mtb* cells treated with 1.0 µM Bio-AMS. The dashed box corresponds to the section of the gel that was excised for trypsin digestion and LC-MS/MS analysis.

(D) Normalized band intensities of bands in lanes 1–3 from (C).

See also Figure S2 and Table S2.

substrate concentrations. As shown in Figure 2A, the half-maximum inhibitor concentration ($IC_{50}$ = 135 ± 9 nM) is approximately equal to half of the enzyme concentration, a characteristic inherent to tight-binding inhibitors (Copeland, 2005). Attempts to determine the true inhibition constant ($K_i$) were complicated by the tight-binding behavior and the bisubstrate nature of inhibition, which precluded assessment by traditional steady-state kinetic methods (Yu et al., 2006).

We employed isothermal titration calorimetry (ITC) to investigate the binding affinity of Bio-AMS for *Mt*BPL. Accurate determinations of the binding constants using ITC are typically limited to a range of $10^3$–$10^8$ $M^{-1}$ (Sigurskjold, 2000). A more reliable approach for determining binding constants greater than $10^8$ $M^{-1}$ is to use displacement ITC in which a high-affinity inhibitor is titrated into a solution of protein that is bound with a weaker ligand (Leavitt and Freire, 2001; Velazquez-Campoy et al., 2001). Displacement ITC experiments were performed (Figure 2B) using biotin as the competitive ligand to obtain values for $K_A$ and $n$ (Experimental Procedures). The binding enthalpy was determined by stoichiometric titration of *Mt*BPL with Bio-AMS at a high $c$ value (Experimental Procedures). The thermodynamic parameters are listed in Table 1. The ITC studies provided an experimental $K_D$ of 0.53 ± 0.13 nM with an $n$ value of 1.12 ± 0.02 indicating one substrate binding site per *MtBPL* monomer. Bio-AMS binds approximately 1700-fold more tightly to *Mt*BPL than biotin (Table 1) (Purushothaman et al., 2008). The binding is solely enthalpically driven ($\Delta H$ = −15.4 ± 0.1 kcal/mol) with an unfavorable entropic component ($-T\Delta S$ = 3.0 ± 0.0 kcal/mol). The large observed enthalpic component is commonly observed among tight-binding bisubstrate inhibitors and can be attributed to numerous hydrogen bonds and electrostatic interactions between inhibitor and protein (Neres et al., 2008; Sikora et al., 2010).

## Antitubercular Activity, Antimicrobial Specificity, and Therapeutic Index

The antitubercular activity of Bio-AMS was evaluated against *Mtb* H37Rv, the common laboratory virulent strain. The minimum inhibitory concentration that inhibited greater than 99% of cell growth ($MIC_{99}$) is 0.31–0.78 µM (Table 2). On the basis of the

**Table 1. Thermodynamic Parameters of Bio-AMS Binding to *Mt*BPL**

| | n | $K_D$, nM | ΔH, kcal mol$^{-1}$ | ΔG, kcal mol$^{-1}$ | −TΔS, kcal mol$^{-1}$ |
|---|---|---|---|---|---|
| Biotin[a] | 0.98 | 940 | −11.1 | −8.1 | 3.0 |
| Bio-AMS | 1.12 ± 0.02 | 0.530 ± 0.134 | −15.4 ± 0.1 | −12.4 ± 0.1 | 3.0 ± 0.0 |

[a] Thermodynamic values for biotin were taken from Purushothaman et al. (2008).

promising antitubercular activity, we then tested Bio-AMS against ten phenotypically characterized MDR and XDR TB strains. The $MIC_{99}$ values range from 0.16 to 0.625 μM (Table 2) demonstrating that Bio-AMS is equally effective against susceptible and MDR- and XDR-TB strains. We also tested the ability of Bio-AMS to inhibit cell growth in other bacterial and fungal strains because BPLs are present in most organisms. Remarkably, Bio-AMS was inactive against a panel of gram-negative bacteria (*A. baumannii*, *E. coli*, *K. pneumoniae* and *P. aeruginosa*,), gram-positive bacteria (*E. faecalis* and *S. aureus*), and fungi (*C. neoformans*, and *C. albicans*) (see Table S1 available online). We speculate the antimicrobial specificity results from limited intracellular accumulation due to differences in cellular penetration and efflux, rather than biochemical selectivity. Because mammals also contain a biotin protein ligase (holocarboxylase synthetase; Campeau and Gravel, 2001), we evaluated the cytotoxicity of Bio-AMS against two mammalian cell lines, Vero cells and DU145 human prostate cells. DU145 cells were insensitive to Bio-AMS, whereas Bio-AMS displayed very low cell cytotoxicity to Vero cells inhibiting 50% growth ($CC_{50}$) at 58 μM providing a therapeutic index ($CC_{50}/MIC_{99}$) of 74–187 on the basis of the MIC against *Mtb* H37Rv.

## Mechanism of Action

To demonstrate that Bio-AMS inhibits protein biotinylation in vivo, a culture of *Mtb* H37Rv was treated with Bio-AMS (0.1 μM or 1.0 μM) along with a DMSO control. After treatment for 26 hr, cells were harvested and lysed. Protein concentrations were determined, and lysates were separated by denaturing gel electrophoresis and imaged via western blot (Figure 2C). The biotinylated protein pattern of the DMSO treated cells (lane 1) shows two biotinylated proteins above 100 kDa, one of which is likely pyruvate carboxylase. Additionally, the proteins between 55–80 kDa are most likely the acyl CoA carboxylases (accA1–A3). Lastly, there is one unidentified biotinylated protein that is approximately 25 kDa. When *Mtb* was incubated with

**Table 2. Biological Activity and Selectivity of Bio-AMS**

| Strain/Cell Line | Resistance Phenotype[a] | Classification[b] | $MIC_{99}$ (μM) | $EC_{50}$ (μM) |
|---|---|---|---|---|
| *M. tuberculosis* H37Rv | Wt | – | 0.31–0.78 | – |
| *M. tuberculosis XDR-1* | HRESPOCTh | XDR | 0.625 | – |
| *M. tuberculosis XDR-2* | HREPKOTh | XDR | 0.625 | – |
| *M. tuberculosis MDR-1* | HRESPO | MDR | 0.16 | – |
| *M. tuberculosis MDR-2* | HREKO | MDR | 0.16 | – |
| *M. tuberculosis MDR-3* | HRESP | MDR | 0.625 | – |
| *M. tuberculosis MDR-4* | HRCPTh | MDR | 0.625 | – |
| *M. tuberculosis MDR-5* | HRERb | MDR | 0.625 | – |
| *M. tuberculosis MDR-6* | HREZSKPTh | MDR | 0.625 | – |
| *M. tuberculosis MDR-7* | HRERb | MDR | 0.625 | – |
| *M. tuberculosis MDR-8* | HREZRbTh | MDR | 0.625 | – |
| *A. baumannii* | - | Gram-negative | >400 | – |
| *E. coli* | - | Gram-negative | >400 | – |
| *K. pneumoniae* | - | Gram-negative | >400 | – |
| *P. aeruginosa* | - | Gram-negative | >400 | – |
| *E. faecalis* | - | Gram-positive | >400 | – |
| *S. aureus* | MRSA | Gram-positive | >400 | – |
| *C. albicans* | - | Fungal | >400 | – |
| *C. neoformans* | - | Fungal | >400 | – |
| DU145 | na | Mammalian | – | >100 |
| Vero | na | Mammalian | – | 58[c] |

The following ATCC strains were used: *A. baumannii*, 19606; *E. coli*, 25922; *K. pneumoniae*, 13883; *P. aeruginosa*, 27853; *E. faecalis*, VRE, 51299; *S. aureus*, MRSE, 43300; *C. albicans*, 10231; *C. neoformans*, 66031. na, not applicable.

[a] Letter codes represent drugs which that strain is resistant to. H = isoniazid; R = rifampicin; E = ethambutol; S = streptomycin; p = para-aminosalicylic acid; O = ofloxacin; Th = thiacetazone; C = capreomycin; K = kanamycin; Rb = rifabutin; Z = pyrazinamide.

[b] XDR = extensively drug-resistant; MDR = multidrug-resistant.

[c] Vero cells were still 25% viable at 500 μM.

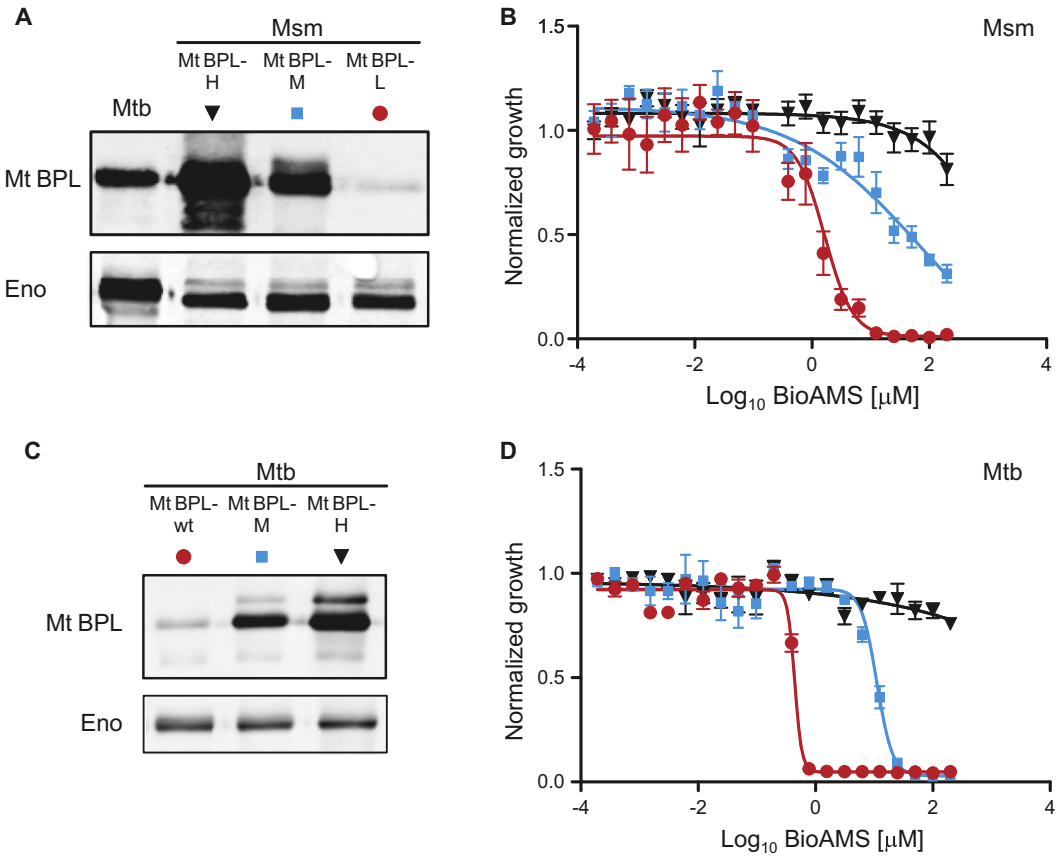


**Figure 3. Impact of *Mt*BPL Expression on Drug Susceptibility of *M. smegmatis* and Mtb**

(A–D) In (A) and (C), 10 μg of total protein extracts of the indicated strains were used to measure *Mt*BPL expression by western blotting. Enolase (lower panels) served as the loading control. (B) and (D) show susceptibility of *M. smegmatis* (*Mt*BPL-H [black], *Mt*BPL-M [blue], and *Mt*BPL-L [red]) and *Mtb* (*Mt*BPL-H [black], *Mt*BPL-M [blue], and *wt* [red]) to BioAMS. Normalized growth was calculated as OD580 at the indicated drug concentration divided by OD580 without drug. Error bars represent SEMs of 4 to 8 measurements.

See also Figures S3–S5.

0.1 μM (~1/3–1/8 × $MIC_{99}$, lane 2), a minimal decrease in band intensity (protein biotinylation) was seen. However, when 1.0 μM Bio-AMS (~1.5–3 × $MIC_{99}$, lane 3) was incubated with *Mtb*, a clear decrease in protein biotinylation of all bands were observed. Band intensities in each lane were calculated and normalized to the amount of protein loaded into each well to provide normalized biotinylation levels (Figure 2D). The biotinylated proteins highlighted by the dashed box in Figure 2C were confirmed to be the acetyl/propionyl CoA carboxylases by mass spectrometry (Figure S2 and Table S2). Because cells were treated with Bio-AMS for only 26 hr before being harvested, the slow doubling time of *Mtb* (24 hr in GAST medium) likely prevented growth arrest in the presence of inhibitor, but still allowed for a measurable decrease in protein biotinylation. These results clearly demonstrate that Bio-AMS decreases global biotinylation levels of proteins involved in fatty acid biosynthesis.

## Validation of the Essentiality of *birA* in *M. smegmatis* and Susceptibility to Inhibition by Bio-AMS

For genetic studies, we first turned to *M. smegmatis*, a fast-growing mycobacterium whose genome encodes homologs for each of the three ACC alpha subunits and the six ACC beta subunits of *Mtb* and that, like the genome of *Mtb*, contains a single BPL-encoding gene (*MsbirA*). After repeated attempts to delete *MsbirA* in wild-type (WT) *M. smegmatis* had failed, we constructed a merodiploid strain, which contained a second *MsbirA* integrated into the attachment site of the phage L5. This allowed us to delete the WT copy of *MsbirA* resulting in *M. smegmatis ΔMsbirA MsbirA*-attL5 (Figures S3 and S4), and to subsequently demonstrate that *M. smegmatis* is unable to form colonies on agar plates without *MsbirA* (Figure S3). We next used *M. smegmatis ΔMsbirA MsbirA*-attL5 to show that the *Mtb birA* gene, *MtbirA*, can replace *MsbirA* and constructed three *M. smegmatis* strains, *Mt*BPL-H, *Mt*BPL-M, and *Mt*BPL-L, which instead of *Ms*BPL express high, intermediate, or low levels of *Mt*BPL, respectively (Figure 3A). These *M. smegmatis* strains all grew normally in liquid media (Figure S5A), but their susceptibility to Bio-AMS increased with decreasing expression of *Mt*BPL (Figure 3B). By contrast, these strains showed identical susceptibilities to isoniazid (INH) and ethambutol (EMB) (Figures S5B and S5C). Next, we generated two *Mtb* strains, *Mtb Mt*BPL-H and *Mt*BPL-M, which overexpressed *Mt*BPL to different degrees (Figure 3C). Overexpression of *Mt*BPL did not affect growth (not shown) or susceptibility of *Mtb* to INH (Figure S5D)

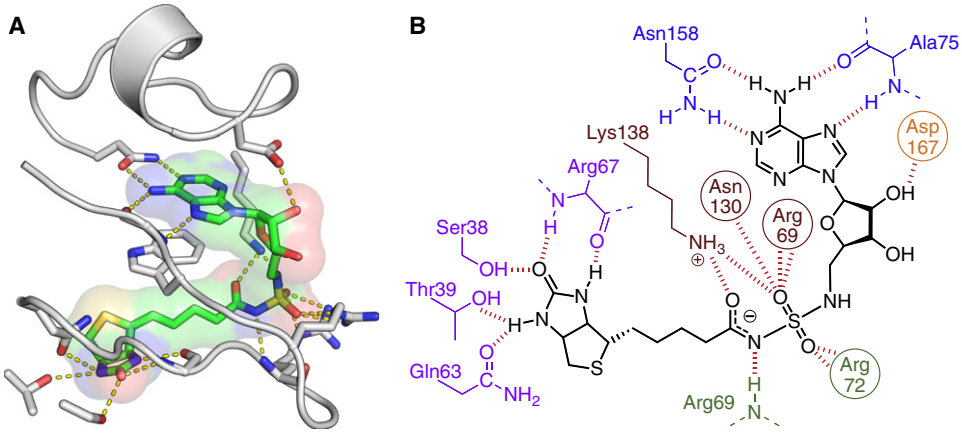


**Figure 4. Structure of Bio-AMS with *Mt*BPL**

(A) The *Mt*BPL binding site showing the loops undergoing the order-to-disorder transition (gray) upon binding of Bio-AMS (green carbons). Specific hydrogen bonds are shown in yellow dashes. Asn130 is omitted for clarity.

(B) Schematic view of polar interactions between biotin (purple), acylsulfamide linker (red/green), ribose (orange), and adenosine (blue) portions of Bio-AMS and *Mt*BPL. See also Figure S6 and Table S3.

but did decrease susceptibility to Bio-AMS (Figure 3D). Taken together, these experiments demonstrated (1) that *MsbirA* is essential for growth of *M. smegmatis*, (2) that *MtbirA* can replace *MsbirA*, and (3) that the BPL expression level specifically determines susceptibility of *M. smegmatis* and *Mtb* to Bio-AMS.

## Cocrystal Structure

To identify important molecular interactions critical to the potency of Bio-AMS, we solved the cocrystal structure with *Mt*BPL to 1.7-Å resolution (see Figure S6 and Table S3 for data collection and refinement statistics). Compared to the apo structures of *Mt*BPL (Gupta et al., 2010; Ma and Wilmanns, 2007), the complex structure reveals that two loops (residues 65–76 and 162–169) undergo a disorder-to-order transition upon binding of Bio-AMS and form extensive, specific contacts (Figure 4), consistent with the displacement ITC results. The biotin moiety and adenine nucleobase are recognized by a common constellation of hydrogen bonds observed in all liganded biotin-protein ligase crystal structures to date (Bagautdinov et al., 2005; Tron et al., 2009; Wood et al., 2006). The adenine nucleobase is specifically recognized via hydrogen bonds with the side chain of Asn158 and backbone of Ala75. Consistent with Bio-AMS being competitive with biotin, the buried urea moiety of biotin is hydrogen bonded to the backbone carbonyl and amide of Arg67, the hydroxyl of Ser38, the side-chain amide of Gln63, and the hydroxyl of Thr39. Analogous to the isosteric 5′-biotinyl-AMP structures reported from *Pyrococcus hiorikoshii* (Bagautdinov et al., 2005), Trp74 packs between the adenine ring and the alkyl tail of biotin. In contrast to all other reported biotin-protein ligase structures, *Mt*BPL possesses a unique interaction between the side-chain amide of Gln81 and both the indole nitrogen of Trp74 and carbonyl of Ala75. Likely unique to *Mt*BPL, Asp167 interacts with the 2′-hydroxyl of the ribose; the only other reported interaction between a ribose hydroxyl and a BPL is seen with Gln221 on a separate portion of the ordered loop with the *Ec*BPL (Wood et al., 2006). With the acylsulfamide linkage, there are extensive interactions between the guanidinium groups of Arg69 and Arg72 and the side chain of Asn130 with the sulfamide oxygens. Because of the low p$K_a$ of the central nitrogen of the acylsulfamide linker, it is likely in the deprotonated amide form; the crystal structure supports this with a hydrogen bond distance of 3.0 Å with good geometry to the backbone N-H of Arg69. The terminal amine of Lys138, which is thought to be critical for adenylation reaction, interacts with and stabilizes the amide oxygen of the acylsulfamide linker, one sulfamide oxygen, the carboxylate of Asp131, and a water molecule that is hydrogen bonded to the distal nitrogen of the sulfamide linkage.

## DISCUSSION

Bio-AMS is considered a bisubstrate inhibitor because it interacts with both substrate (biotin and ATP) binding pockets. Bisubstrate inhibitors (A–B) can realize substantial enhancement in binding energy compared to the sum of the Gibbs binding energies of the respective fragments (A + B) because of a smaller entropy barrier to binding of A–B compared to A + B (Jencks, 1981). Thus, the report that 5′-*O*-[*N*-(biotinyl)sulfamoyl]adenosine **5** bound more weakly than the single substrate biotin was incongruous, particularly in light of several recent reports demonstrating related bisubstrate inhibitors bound with high affinity (Brown and Beckett, 2005; Ferreras et al., 2005; Somu et al., 2006). Competitive displacement isothermal titration calorimetry revealed the true potency of Bio-AMS, providing a $K_D$ of 0.530 nM that is driven exclusively by a large favorable enthalpy of −15.4 kcal/mol. The high affinity and favorable thermodynamic parameters exhibited in the interaction of *Mt*BPL with Bio-AMS correlates well with the detailed molecular interactions observed (Figure 4). The large number of hydrogen bonds and the electrostatic interactions with Lys138 and the backbone of Arg69 result in the large, favorable enthalpy. The conformational restriction of the ligand within the binding pocket, combined with the disorder-to-order transition observed for the two loops of *Mt*BPL covering Bio-AMS, is likely compensated for by the

increased hydrophobic interactions with the alkyl tail of biotin and Trp74 to net only a small unfavorable entropy.

Another important finding from our work was the demonstration that **5** slowly decomposes through cyclonucleoside formation, which has precedent in related 5′-activated nucleosides (Kristinsson et al., 1995; Liang et al., 2008; Yanachkov and Wright, 1994). Replacement of the 5′-oxygen atom in **5** with a nitrogen atom afforded the more stabile acylsulfamide linkage of Bio-AMS. Although the acylsulfamate linkage has historically been used as a bioisostere of the acylphosphate to generate adenylate inhibitors, caution is warranted because of its potential lack of stability. Several strategies exist to improve the stability including replacement of the 5′-oxygen with a nitrogen atom as shown herein or a carbon atom. Alternate strategies to prevent the undesired cyclonucleoside formation include installation of a bulky group at the C-2 position of the adenine ring to hinder the required *syn* conformation about the glycosidic linkage or deletion of the N-3 nitrogen atom of adenine to prevent nucleophilic attack. As demonstrated in this work, the replacement of the 5′ oxygen with a nitrogen provides the required stability while maintaining isostere integrity.

The observation that Bio-AMS exhibited potent whole-cell activity toward *Mtb* was unexpected. Indeed, related acyladenylate bisubstrate inhibitors developed for the functionally related aminoacyl tRNA synthetases have typically been devoid of whole-cell activity owing to the limited membrane permeability of these highly polar nucleoside analogs (Hurdle et al., 2005; Kim et al., 2003; Pohlmann and Brötz-Oesterhelt, 2004). Mycobacteria are considered to have the most complex and fortified cellular wall of any bacterial species; thus, the potent and selective antitubercular activity was intriguing. However, the ability of these bisubstrate adenylate inhibitors to cross the cell wall of *Mtb* is not unprecedented, because our laboratory and others have shown that these inhibitors possess potent whole-cell antitubercular activity (Ferreras et al., 2005; Somu et al., 2006). We hypothesize that the observed selectivity is likely due to selective accumulation facilitated by one of the ~30 ATP-binding cassette (ABC) transporters present in *Mtb* (Braibant et al., 2000) that are responsible for assimilation of nucleosides and cofactors.

Biotinylation, catalyzed by the mycobacterial biotin protein ligase *Mt*BPL, is a posttranslation modification that represents a key nodal point in mycobacterial fatty acid metabolism and controls flux through both fatty acid biosynthetic and catabolic pathways. We designed and synthesized the bisubstrate inhibitor Bio-AMS, which was shown by isothermal titration calorimetry to bind *Mt*BPL with a subnanomalor dissociation constant. Despite its highly polar structure, Bio-AMS also displayed impressive whole-cell activity against *Mtb* H37Rv, as well as a panel of MDR and XDR *Mtb* strains. The selective antitubercular activity of this compound is intriguing and may be the result of selective mycobacterial accumulation. Further biochemical and cell-based accumulation studies will be required to delineate the origin of the remarkable selective antitubercular activity. Nevertheless, our genetic experiments with *M. smegmatis* demonstrated that *MsbirA* is an essential gene and also confirmed that the antibacterial activity of Bio-AMS is BPL dependent. Proteomic analysis demonstrated that Bio-AMS also inhibits protein biotinylation in *Mtb*. The detailed molecular interactions visualized in the cocrystal structure of *Mt*BPL with Bio-AMS pinpoint key opportunities to engineer selectivity and further augment binding affinity. Thus, the work presented here validates *Mt*BPL as an attractive target for the development of novel antitubercular agents. Beyond their role as potential antitubercular agents, Bio-AMS may also find utility as tool compound for chemical biology studies because biotinylation is widely used for site-specific protein labeling and other biotechnological applications.

## SIGNIFICANCE

**With the rapid emergence of drug-resistant strains of *Mycobacterium tuberculosis* comes the need to identify new drug targets and develop small molecule inhibitors for these enzymes. Here, we synthesized a potent bisubstrate inhibitor for studying a promising enzyme target from *Mtb*. In designing this inhibitor, we have identified an important decomposition mechanism among bisubstrate adenylation inhibitors, indicating that careful attention needs to be given to engineering stability into these small molecules. The cocrystal structure of the inhibitor-bound BPL enzyme provides key insight into the structural differences between BPL from *Mtb* and other organisms, which builds the foundation for future medicinal chemistry efforts. Additionally, these studies use genetic knockdowns to determine the mechanism of action of a new small molecule probe in mycobacteria. Lastly, our genetic knockout results demonstrate that BPL is an essential enzyme, further validating this enzyme as a promising candidate target for antibiotic development.**

## EXPERIMENTAL PROCEDURES

See Supplemental Information for full synthetic procedures, cloning and expression of *Mt*BPL, antimicrobial and cytotoxicity assays, and biotinylated protein identification.

### Bio-AMS Synthesis

Bio-AMS was synthesized in two steps starting from 5′-amino-5′-*N*-*tert*-butoxycarbonyl-5′-deoxy-2′,3′-*O*-isopropylidene-5′-*N*-(sulfamoyl)adenosine (**S5** (Lu et al., 2008), Supplemental Scheme S3) in 55% overall yield. Biotin was coupled to **S5** (Lu et al., 2008) followed by global TFA deprotection to yield crude Bio-AMS (**6**). The title compound was purified by reverse phase HPLC. Detailed experimental procedures are provided in the Supplemental Information: $^{1}$H NMR (600 MHz, DMSO-$d_6$) δ 0.96 (t, *J* = 4.8 Hz, 18H, 2 equiv. TEA), 1.22–1.33 (m, 2H), 1.39–1.50 (m, 3H), 1.57–1.63 (m, 1H), 2.08 (t, *J* = 7.2 Hz, 2H), 2.49 (p, *J* = 1.8 Hz, 9H, 2 equiv. TEA), 2.56 (d, *J* = 5.4 Hz, 1H), 2.79 (dd, *J* = 12.6, 4.8 Hz, 1H), 3.05 (ddd, *J* = 8.4, 6.1, 4.7 Hz, 1H), 3.09 (dd, *J* = 13.2, 4.2 Hz, 2H), 4.03 (dd, *J* = 7.2, 4.2 Hz, 1H), 4.09–4.11 (m, 2H), 4.26 (dd, *J* = 7.8, 5.4 Hz, 1H), 4.68 (q, *J* = 4.8 Hz, 1H), 5.25 (s, 1H) 5.43 (d, *J* = 6.0 Hz, 1H), 5.82 (d, *J* = 6.6 Hz, 1H), 6.34 (s, 1H), 6.52 (s, 1H), 7.38 (s, 2H), 8.18 (s, 1H), 8.29 (s, 1H); $^{13}$C NMR (150 MHz, $CD_3OD$) δ 11.7, 25.7, 28.5, 28.7, 37.3, 40.5, 45.8, 46.2, 55.8, 59.6, 61.5, 71.8, 73.1, 84.1, 88.5, 119.9, 140.7, 149.4, 153.0, 156.7, 163.2, 173.2; HRMS (ESI–) calcd for $C_{20}H_{28}N_9O_7S_2$ $[M - H]^-$ 570.1559, found 570.1523 (error 6.3 ppm).

### Kinetic Inhibition Assays

Enzyme assays to determine the $IC_{50}$ value for Bio-AMS were run under initial velocity conditions using our recently described coupled adenylation–hydroxamate formation assay employing saturating concentrations of both ATP and biotin (Wilson and Aldrich, 2010). Varying concentrations of inhibitor Bio-AMS (20 mM DMSO stock), providing a final DMSO concentration of 1% (v/v), or

DMSO only (control) were preincubated with a master mix (250 nM *Mt*BPL, 50 mM Tris [pH 8.0}, 5.0 mM $MgCl_2$, 0.5 mM DTT, 2.5 mM ATP, 0.1 unit of nucleoside phosphorylase, 0.04 unit of pyrophosphatase, 0.2 mM 7-methylthioguanosine [MesG], and 150 mM hydroxylamine [pH 7.0]) for 10 min at 25°C. The master mix (95 μL) was then added to 5.0 μl of a biotin solution to provide a final biotin concentration of 250 μM. Reactions (100 μL) were run in 96-well half-area UVStar plates (Greiner), and the formation of 7-methyl-6-thioguanine was measured at 360 nm ($\varepsilon_{360}$ = 11,000 $mol^{-1}$ $cm^{-1}$) at 25°C on a Molecular Devices SpectraMax M5e. The initial velocity data were fit by nonlinear regression analysis to the sigmoidal Hill equation (Equation 1), as follows:

$$\frac{v_i}{v_0} = B + \frac{A - B}{1 + 10^{(\log C_{50} - I) \times h}}, \quad (1)$$

using GraphPad prism version 4.0 to obtain the $IC_{50}$ value, where $v_i/v_0$ is the initial fractional velocity, $h$ is the Hill slope, $I$ is the logarithm of the inhibitor concentration, and $A$ and $B$ are the top and bottom of the curve, respectively.

### Isothermal Titration Calorimetry

ITC experiments were conducted on a Microcal VP-ITC microcalorimeter (Northhampton, MA). All titration experiments were performed at 20°C in ITC buffer (10 mM Tris [pH 7.5], 200 mM KCl, and 2.5 mM $MgCl_2$). *Mt*BPL was exchanged into ITC buffer using an Amicon Ultra concentrator (Millipore, Billerica, MA, USA), and final enzyme concentrations were determined using an $\varepsilon_{280}$ of 35540 $M^{-1}$ $cm^{-1}$. In individual titrations, ligands were injected into solutions of the enzyme. The quantity $c = K_A M_t(0)$, in which $M_t(0)$ is the initial enzyme concentration is crucial for successful ITC experiments (Wiseman et al., 1989). Experiments for the determination of $\Delta H$ (the change in binding enthalpy in kilocalories per mole) were performed with a $c$ value in the range of 1.2–2.4 × $10^4$, while displacement ITC experiments were performed with a $c$ value in the range of 206–415. Ligand and protein concentrations for the determination of $\Delta H$ were 16 μM *Mt*BPL and 160 μM Bio-AMS. The $K_A$ (the association constant in $M^{-1}$) and $n$ (the number of binding sites per monomer) values were determined by ITC displacement experiments with 150 μM biotin added to both the enzyme and ligand solutions. Enzyme concentrations for displacement experiments were increased to 42 μM for titration with 420 μM Bio-AMS. All titrations were performed in duplicate using a stirring speed of 307 rpm and a 300 s interval between 10 μl injections. The first injection was omitted from data fitting. Titrations were run past the enzyme saturation point to correct for heats of dilution. The data for the stoichiometric titration of Bio-AMS in *Mt*BPL provided $\Delta H$ values. The experimental data for the competitive displacement ITC experiments were fitted to a theoretical titration curve using the Origin software package (version 7.0) to provide $K_A^{app}$ and $n$ values (Velazquez-Campoy and Freire, 2006). The $K_A$ value for Bio-AMS was obtained from the $K_A^{app}$ value using Equation 2:

$$K_A = K_A^{app}\left(1 + K_A^B[B]\right), \quad (2)$$

where [$B$] ([biotin]) equals 150 μM and $K_A^B$ (association constant for biotin) = 1.08 × $10^6$. The thermodynamic parameters (ΔG and –TΔS) were calculated using Equation 3:

$$\Delta G = -RT \ln K = \Delta H - T\Delta S, \quad (3)$$

where $\Delta G$, $\Delta H$, and $\Delta S$ are the changes in free energy, enthalpy, and entropy of binding, respectively, $R$ = 1.98 cal $mol^{-1}$ $K^{-1}$, and $T$ is the absolute temperature. The affinity of Bio-AMS for *Mt*BPL is provided as the dissociation constant ($K_D = 1/K_A$). Direct and competitive ITC experiments were performed in two independent experiments and analyzed independently. The thermodynamic values were then averaged. ITC experiments for determining the binding affinity of biotin ($K_A^B$ in Equation 2) for *Mt*BPL were performed as described above. Ligand and enzyme concentrations were 195 μM and 19.5 μM, respectively. The data were then fit using the single-site binding model provided in Origin 7.0 to determine $K_A^B$.

### Antitubercular Assays

For determination of minimum inhibitory concentrations (MICs) against *Mtb* strains, broth microdilution assays were determined in quadruplicate in GAST media supplemented with $Fe^{3+}$ (De Voss et al., 2000) using Bio-AMS from a DMSO stock solution or with control wells treated with an equivalent volume of DMSO or with isoniazid as positive control. Cells were grown to an $OD_{650}$ of 0.2, diluted 1000-fold in the GAST/Fe medium and 50 μl added per well of a 96-well plate containing 50 μl of GAST/Fe medium with compound in a two-fold dilution series across the wells giving an initial cell density of $10^4$ cells/well. Plates were incubated at 37°C, and growth was monitored at 7 and 14 days. The MIC was recorded as the lowest concentration of compound that resulted in complete inhibition of growth. MICs were determined against the laboratory strain *Mtb* H37Rv as well as a panel of drug-resistant clinical isolates of *Mtb* (Jeon et al., 2008).

### Biotinylated Proteome Assay

A 30 ml culture of *Mtb* H37Rv was grown at 37°C to an $OD_{650}$ of 0.194, and was split into 3 × 10 mL. The 10 ml cultures were treated with either 0.1 μM DMSO or 1.0 μM Bio-AMS for 26 hr at 37°C. After this time, the $OD_{650}$ values for the DMSO and 1.0 μM treated cells were 0.616 and 0.600, respectively. The cells were harvested and the cell pellets were washed once with PBS (10 mM sodium phosphate and 150 mM NaCl [pH 7.8]) and were frozen at −80°C. The cells were subjected to bead beating in PBS containing protease inhibitor cocktail (Roche). After removing unlysed cells and cell wall debris by centrifuging, the total protein concentrations were determined for the 0.1 μM DMSO and 1.0 μM Bio-AMS-treated cells and were found to be 2.0, 2.2, and 2.2 mg/mL, respectively. An equal volume of 2× SDS reducing gel electrophoresis loading buffer was added to the samples, which were subsequently heated for 10 min at 80°C. A 5.0 μl aliquot of each sample was separated by denaturing gel electrophoresis (4%–15% Tris-HCl Ready Gel, BioRad) and was transferred to a PVDF membrane (iBlot System, Invitrogen). The membrane was blocked with Tris-buffered saline containing 0.05% Tween-20 (TBST) containing 1.0% BSA for 30 min at 25°C. The membrane was incubated with an AlexaFluor 647 fluorescent-streptavidin conjugate (Invitrogen) at a dilution of 1:1000 in TBST for 1 hr at 25°C, after which the membrane was washed 3 × 10 ml TBST. Biotinylated proteins within the membrane were visualized by fluorescence scanning using an FMBIO III fluorescent scanner (MaraiBio). Band intensities were calculated using the Image Analysis software version 3.0 provided with the scanner. Band intensities were normalized for protein concentration to provide the normalized percentage band intensity values in Figure 2D.

### Essentiality of *birA*

For mutant construction, *Mycobacterium smegmatis* $mc^2155$ was grown at 37°C on Difco 7H11 agar (BD) or in Difco Middlebrook 7H9 broth (BD) with 0.2% v/v glycerol and 0.05% v/v Tween 80. Antibiotics were added, where appropriate, at 50 μg/ml (hygromycin B, Calbiochem), 20 μg/ml (streptomycin, Sigma), 25 μg/ml (kanamycin A, Sigma), or 25 μg/ml (zeocin, Invitrogen). Preparation of competent cells, electroporations, and the preparation of genomic DNAs were performed as described elsewhere (Ehrt et al., 2005). Plasmids were constructed using standard procedures (details are available upon request). Polyclonal anti-*Mt*BPL antibodies were generated using a commercial immunization service (Covance).

Initially, we attempted to delete *MsbirA* from the chromosome of *M. smegmatis* and cloned a knockout plasmid, pKO-*MsbirA* (derived from pSM270; Manganelli et al., 2001) in which ~800 bp DNA fragments containing the upstream and downstream region of *MsbirA* were separated by a hygromycin resistance gene. Integration of pKO-*MsbirA* into the *M. smegmatis* chromosome by a single crossover conferred resistance to hygromycin (hygR) and streptomycin (strepR) as well as sensitivity to sucrose (sucS). A second crossover that would have deleted *MsbirA* would have resulted in a strain that is hygR, streptomycin sensitive, and sucrose resistant. We analyzed 150 sucrose-resistant descendants of two different single crossover strains, but were unable to identify a single *MsbirA* deletion mutant among them. This strongly suggested that *MsbirA* is essential for growth of *M. smegmatis*.

We next constructed a *birA* merodiploid (Figure S3, step 1) by transforming *M. smegmatis* with a kanamycin resistance (kanR) conferring *MsbirA* expression plasmid that integrated into the attachment site of the mycobacteriophage L5 (attL5). Deletion of the WT copy of *MsbirA* in the merodiploid (Figure S3, step 2) with pKO-*MsbirA* proved to be straightforward and was confirmed by southern blotting (Figure S4). We refer to the resulting strain as *ΔMsbirA MsbirA*-attL5 to indicate that the only functional copy of *MsbirA* is

located in the attL5-site. Plasmids in the attL5 site can be efficiently replaced by site-specific recombination (Pashley and Parish, 2003), which allowed us to determine whether *M. smegmatis* is able to grow after deletion of *MsbirA*. Replacement of the kanR *MsbirA* expression plasmid with a zeocin resistance (zeoR) conferring plasmid that contained *MsbirA* was efficient (Figure S3, step 4). In contrast, no zeoR colonies were obtained in several independent transformations of *ΔMsbirA MsbirA*-attL5 with a zeoR plasmid that did not contain *MsbirA* (Figure S3, step 3). This demonstrated that deletion of *MsbirA* prevents growth of *M. smegmatis* on agar plates.

To generate *M. smegmatis* mutants that expressed *Mt*BPL instead of *Ms*BPL we transformed *ΔbirA MsbirA*-attL5 with zeoR plasmids containing *MtbirA*. Mutants in which *MsbirA*-attL5 was replaced by *MtbirA*-attL5 were identified by confirming sensitivity to kanamycin (which is a result of deleting the *MsbirA* plasmid from the attL5) and in immunoblots performed with a polyclonal antibody that was generated against *Mt*BPL and did not recognize *Ms*BPL. Plasmids that contained different promoters upstream of *MtbirA* were used to generate strains that constitutively expressed different levels of *Mt*BPL (Figure 3A). Transformation of plasmids in which (1) the native upstream region of *MtbirA*, (2) the promoter Psmyc (Kaps et al., 2001), or (3) Ptb38 were used to transcribe *MtbirA* yielded *Msm Mt*BPL-L, *Msm Mt*BPL-M, and *Msm Mt*BPL-M, respectively. Promoter Ptb38 is contained within a DNA fragment that has been identified in a promoter trap screen (Ehrt et al., 2005). This promoter has strong activity in *M. smegmatis* and slightly lower activity in *Mtb* (unpublished data). Plasmids containing *MtbirA* transcribed by Ptb38 and Psmyc were transformed in *Mtb* H37Rv to generate *Msm Mt*BPL-M and *Msm Mt*BPL-M, respectively. The Enolase was used as loading control and was detected using a polyclonal antibody provided by Dr. Sabine Ehrt. All *M. smegmatis* mutants in which *MsbirA* was replaced by *MtbirA* grew similarly to WT *M. smegmatis* (Figure S5). Overexpression of *Mt*BPL also did not affect growth of *Mtb* (data not shown). The activity of Bio-AMS against the *M. smegmatis* strains was assessed as described for *Mtb* with two exceptions: growth was analyzed after 2 to 4 days instead of 10 to 14 days and no iron supplement was added to the GAST medium.

### Crystallization

BirA was incubated with a slight molar excess of Bio-AMS for 30 min at 37°C prior to crystallization. Crystals were grown in 1–2 weeks at 20°C by microseeding with apo crystals in hanging drops using the vapor-diffusion method. The protein solution contained 4.6 mg/mL BirA, 10 mM HEPES (pH 7.5), 50 mM NaCl, 1 mM DTT, 1.05% DMSO, and 200 μM Bio-AMS. Equal volumes were mixed of protein solution and mother liquor containing 20% MPEG 2000, 50 mM trimethylamine *N*-oxide, and 100 mM Tris (pH 8.5). Crystals were cryo-protected in a solution containing mother liquor supplemented with 20% PEG 400 and flash frozen in liquid nitrogen.

### Data Collection and Structure Solution

X-ray diffraction data were collected at 100 K and 1.000 Å wavelength on beamline 4.2.2 at the Advanced Light Source, Berkeley, CA. Data were integrated and scaled by d*TREK (Pflugrath, 1999). The structure was solved by molecular replacement using the previously determined apo *Mt*BPL structure (PDB code 2CGH) and the program Phaser (McCoy et al., 2007) from within CCP4 (Collaborative Computational Project, 1994). Initial refinement and manual model rebuilding was performed using REFMAC5 (Murshudov et al., 1997) and Coot (Emsley and Cowtan, 2004), respectively. Topology and parameter files for Bio-AMS were generated using the PRODRG server (Schüttelkopf and van Aalten, 2004). Final refinement was performed using Phenix (Adams et al., 2010). Ramachandran plots were calculated by MOLPROBITY and showed 96.4% of the residues were in the favored regions and all residues were in the allowed regions. OMIT density (Figure S6) was calculated using the program SFCHECK (Vaguine et al., 1999). Images and figures were prepared using PyMOL (DeLano Scientific, Palo Alto, CA, USA).

## ACCESSION NUMBER

The atomic coordinates and structure factors were deposited with the Protein Data Bank with the accession code 3RUX.

## SUPPLEMENTAL INFORMATION

Supplemental Information includes six figures, three tables, and Supplemental Experimental Procedures and may be found with this article online at doi:10.1016/j.chembiol.2011.08.013.

## ACKNOWLEDGMENTS

This research was supported by the National Institutes of Health (Grant AI-091790 to D.S. and C.C.A.), the Bill and Melinda Gates Foundation and the Wellcome Trust through the Grand Challenges in Global Health Initiative (support to Douglas Young, Imperial College), and the Intramural Research Program of the National Institutes of Health National Institute of Allergy and Infectious Disease (support to C.E.B.). We thank Dr. Sabine Ehrt for enolase specific antiserum, Dr. Christine Salomon and Mr. Michael Donald for antimicrobial specificity testing, and Dr. David Ferguson and Mr. Adam Benoit for DU145 cell testing.

Received: May 23, 2011
Revised: August 5, 2011
Accepted: August 24, 2011
Published: November 22, 2011

## REFERENCES

Adams, P.D., Afonine, P.V., Bunkóczi, G., Chen, V.B., Davis, I.W., Echols, N., Headd, J.J., Hung, L.W., Kapral, G.J., Grosse-Kunstleve, R.W., et al. (2010). PHENIX: a comprehensive Python-based system for macromolecular structure solution. Acta Crystallogr. D Biol. Crystallogr. *66*, 213–221.

Bagautdinov, B., Kuroishi, C., Sugahara, M., and Kunishima, N. (2005). Crystal structures of biotin protein ligase from *Pyrococcus horikoshii* OT3 and its complexes: structural basis of biotin activation. J. Mol. Biol. *353*, 322–333.

Braibant, M., Gilot, P., and Content, J. (2000). The ATP binding cassette (ABC) transport systems of *Mycobacterium tuberculosis*. FEMS Microbiol. Rev. *24*, 449–467.

Broeckaert, L., Moens, J., Roos, G., De Proft, F., and Geerlings, P. (2008). Intrinsic nucleofugality scale within the framework of density functional reactivity theory. J. Phys. Chem. A *112*, 12164–12171.

Brown, P.H., and Beckett, D. (2005). Use of binding enthalpy to drive an allosteric transition. Biochemistry *44*, 3112–3121.

Brown, P.H., Cronan, J.E., Grøtli, M., and Beckett, D. (2004). The biotin repressor: modulation of allostery by corepressor analogs. J. Mol. Biol. *337*, 857–869.

Campeau, E., and Gravel, R.A. (2001). Expression in *Escherichia coli* of N- and C-terminally deleted human holocarboxylase synthetase: influence of the N-terminus on biotinylation and identification of a minimum functional protein. J. Biol. Chem. *276*, 12310–12316.

Chapman-Smith, A., and Cronan, J.E., Jr. (1999). The enzymatic biotinylation of proteins: a post-translational modification of exceptional specificity. Trends Biochem. Sci. *24*, 359–363.

Collaborative Computational Project, Number 4. (1994). The CCP4 suite: programs for protein crystallography. Acta Crystallogr. D Biol. Crystallogr. *50*, 760–763.

Copeland, R.A., ed. (2005). Evaluation of enzyme inhibitors in drug discovery (New Jersey: John Wiley & Sons, Inc.).

De Voss, J.J., Rutter, K., Schroeder, B.G., Su, H., Zhu, Y., and Barry, C.E., 3rd. (2000). The salicylate-derived mycobactin siderophores of *Mycobacterium tuberculosis* are essential for growth in macrophages. Proc. Natl. Acad. Sci. USA *97*, 1252–1257.

Ehrt, S., Guo, X.V., Hickey, C.M., Ryou, M., Monteleone, M., Riley, L.W., and Schnappinger, D. (2005). Controlling gene expression in mycobacteria with anhydrotetracycline and Tet repressor. Nucleic Acids Res. *33*, e21.

Emsley, P., and Cowtan, K. (2004). Coot: model-building tools for molecular graphics. Acta Crystallogr. D Biol. Crystallogr. *60*, 2126–2132.

 

Ferreras, J.A., Ryu, J.S., Di Lello, F., Tan, D.S., and Quadri, L.E. (2005). Small-molecule inhibition of siderophore biosynthesis in *Mycobacterium tuberculosis* and *Yersinia pestis*. Nat. Chem. Biol. *1*, 29–32.

Gago, G., Kurth, D., Diacovich, L., Tsai, S.C., and Gramajo, H. (2006). Biochemical and structural characterization of an essential acyl coenzyme A carboxylase from *Mycobacterium tuberculosis*. J. Bacteriol. *188*, 477–486.

Gupta, V., Gupta, R.K., Khare, G., Salunke, D.M., Surolia, A., and Tyagi, A.K. (2010). Structural ordering of disordered ligand-binding loops of biotin protein ligase into active conformations as a consequence of dehydration. PLoS ONE *5*, e9222.

Hurdle, J.G., O'Neill, A.J., and Chopra, I. (2005). Prospects for aminoacyl-tRNA synthetase inhibitors as new antimicrobial agents. Antimicrob. Agents Chemother. *49*, 4821–4833.

Jencks, W.P. (1981). On the attribution and additivity of binding energies. Proc. Natl. Acad. Sci. USA *78*, 4046–4050.

Jeon, C.Y., Hwang, S.H., Min, J.H., Prevots, D.R., Goldfeder, L.C., Lee, H., Eum, S.Y., Jeon, D.S., Kang, H.S., Kim, J.H., et al. (2008). Extensively drug-resistant tuberculosis in South Korea: risk factors and treatment outcomes among patients at a tertiary referral hospital. Clin. Infect. Dis. *46*, 42–49.

Kaps, I., Ehrt, S., Seeber, S., Schnappinger, D., Martin, C., Riley, L.W., and Niederweis, M. (2001). Energy transfer between fluorescent proteins using a co-expression system in *Mycobacterium smegmatis*. Gene *278*, 115–124.

Kim, S., Lee, S.W., Choi, E.C., and Choi, S.Y. (2003). Aminoacyl-tRNA synthetases and their inhibitors as a novel family of antibiotics. Appl. Microbiol. Biotechnol. *61*, 278–288.

Kristinsson, H., Nebel, K., O'Sullivan, A.C., Pachlatko, J.P., and Yamaguchi, Y. (1995). Herbically Active Sulfamoyl Nucleosides. In Synthesis and chemistry of agrochemicals IV, D.R. Baker, J.G. Fenyes, and G.S. Basarab, eds. (Washington, D.C.: ACS Publications).

Kurth, D.G., Gago, G.M., de la Iglesia, A., Bazet Lyonnet, B., Lin, T.W., Morbidoni, H.R., Tsai, S.C., and Gramajo, H. (2009). ACCase 6 is the essential acetyl-CoA carboxylase involved in fatty acid and mycolic acid biosynthesis in mycobacteria. Microbiology *155*, 2664–2675.

Leavitt, S., and Freire, E. (2001). Direct measurement of protein binding energetics by isothermal titration calorimetry. Curr. Opin. Struct. Biol. *11*, 560–566.

Liang, F., Jain, N., Hutchens, T., Shock, D.D., Beard, W.A., Wilson, S.H., Chiarelli, M.P., and Cho, B.P. (2008). Alpha,beta-methylene-2′-deoxynucleoside 5′-triphosphates as noncleavable substrates for DNA polymerases: isolation, characterization, and stability studies of novel 2′-deoxycyclonucleosides, 3,5′-cyclo-dG, and 2,5′-cyclo-dT. J. Med. Chem. *51*, 6460–6470.

Lu, X., Zhang, H., Tonge, P.J., and Tan, D.S. (2008). Mechanism-based inhibitors of MenE, an acyl-CoA synthetase involved in bacterial menaquinone biosynthesis. Bioorg. Med. Chem. Lett. *18*, 5963–5966.

Ma, Q., and Wilmanns, M. (2007). Protein Data Bank code 2CGH. http://www.rcsb.org/pdb/explore/explore.do?structureId=2CGH. Accessed July 28, 2011.

Manganelli, R., Voskuil, M.I., Schoolnik, G.K., and Smith, I. (2001). The *Mycobacterium tuberculosis* ECF sigma factor sigmaE: role in global gene expression and survival in macrophages. Mol. Microbiol. *41*, 423–437.

Marrero, J., Rhee, K.Y., Schnappinger, D., Pethe, K., and Ehrt, S. (2010). Gluconeogenic carbon flow of tricarboxylic acid cycle intermediates is critical for *Mycobacterium tuberculosis* to establish and maintain infection. Proc. Natl. Acad. Sci. USA *107*, 9819–9824.

McCoy, A.J., Grosse-Kunstleve, R.W., Adams, P.D., Winn, M.D., Storoni, L.C., and Read, R.J. (2007). Phaser crystallographic software. J. Appl. Cryst. *40*, 658–674.

Murshudov, G.N., Vagin, A.A., and Dodson, E.J. (1997). Refinement of macromolecular structures by the maximum-likelihood method. Acta Crystallogr. D Biol. Crystallogr. *53*, 240–255.

Neres, J., Labello, N.P., Somu, R.V., Boshoff, H.I., Wilson, D.J., Vannada, J., Chen, L., Barry, C.E., 3rd, Bennett, E.M., and Aldrich, C.C. (2008). Inhibition of siderophore biosynthesis in *Mycobacterium tuberculosis* with nucleoside bisubstrate analogues: structure-activity relationships of the nucleobase domain of 5′-O-[N-(salicyl)sulfamoyl]adenosine. J. Med. Chem. *51*, 5349–5370.

Pashley, C.A., and Parish, T. (2003). Efficient switching of mycobacteriophage L5-based integrating plasmids in *Mycobacterium tuberculosis*. FEMS Microbiol. Lett. *229*, 211–215.

Pflugrath, J.W. (1999). The finer things in X-ray diffraction data collection. Acta Crystallogr. D Biol. Crystallogr. *55*, 1718–1725.

Pohlmann, J., and Brötz-Oesterhelt, H. (2004). New aminoacyl-tRNA synthetase inhibitors as antibacterial agents. Curr. Drug Targets Infect. Disord. *4*, 261–272.

Portevin, D., de Sousa-D'Auria, C., Montrozier, H., Houssin, C., Stella, A., Lanéelle, M.A., Bardou, F., Guilhot, C., and Daffé, M. (2005). The acyl-AMP ligase FadD32 and AccD4-containing acyl-CoA carboxylase are required for the synthesis of mycolic acids and essential for mycobacterial growth: identification of the carboxylation product and determination of the acyl-CoA carboxylase components. J. Biol. Chem. *280*, 8862–8874.

Purushothaman, S., Gupta, G., Srivastava, R., Ramu, V.G., and Surolia, A. (2008). Ligand specificity of group I biotin protein ligase of *Mycobacterium tuberculosis*. PLoS ONE *3*, e2320.

Schüttelkopf, A.W., and van Aalten, D.M. (2004). PRODRG: a tool for high-throughput crystallography of protein-ligand complexes. Acta Crystallogr. D Biol. Crystallogr. *60*, 1355–1363.

Sigurskjold, B.W. (2000). Exact analysis of competition ligand binding by displacement isothermal titration calorimetry. Anal. Biochem. *277*, 260–266.

Sikora, A.L., Wilson, D.J., Aldrich, C.C., and Blanchard, J.S. (2010). Kinetic and inhibition studies of dihydroxybenzoate-AMP ligase from *Escherichia coli*. Biochemistry *49*, 3648–3657.

Slayden, R.A., Lee, R.E., and Barry, C.E., 3rd. (2000). Isoniazid affects multiple components of the type II fatty acid synthase system of *Mycobacterium tuberculosis*. Mol. Microbiol. *38*, 514–525.

Somu, R.V., Boshoff, H., Qiao, C., Bennett, E.M., Barry, C.E., 3rd, and Aldrich, C.C. (2006). Rationally designed nucleoside antibiotics that inhibit siderophore biosynthesis of *Mycobacterium tuberculosis*. J. Med. Chem. *49*, 31–34.

Timm, J., Post, F.A., Bekker, L.G., Walther, G.B., Wainwright, H.C., Manganelli, R., Chan, W.T., Tsenova, L., Gold, B., Smith, I., et al. (2003). Differential expression of iron-, carbon-, and oxygen-responsive mycobacterial genes in the lungs of chronically infected mice and tuberculosis patients. Proc. Natl. Acad. Sci. USA *100*, 14321–14326.

Tron, C.M., McNae, I.W., Nutley, M., Clarke, D.J., Cooper, A., Walkinshaw, M.D., Baxter, R.L., and Campopiano, D.J. (2009). Structural and functional studies of the biotin protein ligase from *Aquifex aeolicus* reveal a critical role for a conserved residue in target specificity. J. Mol. Biol. *387*, 129–146.

Vaguine, A.A., Richelle, J., and Wodak, S.J. (1999). SFCHECK: a unified set of procedures for evaluating the quality of macromolecular structure-factor data and their agreement with the atomic model. Acta Crystallogr. D Biol. Crystallogr. *55*, 191–205.

Velazquez-Campoy, A., and Freire, E. (2006). Isothermal titration calorimetry to determine association constants for high-affinity ligands. Nat. Protoc. *1*, 186–191.

Velazquez-Campoy, A., Kiso, Y., and Freire, E. (2001). The binding energetics of first- and second-generation HIV-1 protease inhibitors: implications for drug design. Arch. Biochem. Biophys. *390*, 169–175.

Wilson, D.J., and Aldrich, C.C. (2010). A continuous kinetic assay for adenylation enzyme activity and inhibition. Anal. Biochem. *404*, 56–63.

Wiseman, T., Williston, S., Brandts, J.F., and Lin, L.N. (1989). Rapid measurement of binding constants and heats of binding using a new titration calorimeter. Anal. Biochem. *179*, 131–137.

Wood, Z.A., Weaver, L.H., Brown, P.H., Beckett, D., and Matthews, B.W. (2006). Co-repressor induced order and biotin repressor dimerization: a case for divergent followed by convergent evolution. J. Mol. Biol. *357*, 509–523.

Yanachkov, I.B., and Wright, G.E. (1994). Amino-imino tautomerization of *N*2-(4-*n*-butylphenyl)-2′-deoxy-3,5′-cycloguanosine. J. Org. Chem. *59*, 6739–6743.

Yu, M., Magalhães, M.L., Cook, P.F., and Blanchard, J.S. (2006). Bisubstrate inhibition: theory and application to N-acetyltransferases. Biochemistry *45*, 14788–14794.